

Measurement of the Muon Flux at SND@LHC

Results from the 2023-2025 Proton and Heavy-Ion Periods

The SND@LHC Collaboration^{a,1}

¹Full authorlist at the end of the article.

Received: date / Accepted: date

Abstract The SND@LHC experiment investigates neutrinos in the forward pseudorapidity range of $7.2 < \eta < 8.4$. The detector consists of a veto system, a scintillating fiber (SciFi) tracker interleaved with emulsion cloud chambers (ECCs), and a downstream muon system. Muons originating from collisions at ATLAS (IP1) constitute the primary background for CC neutrino interactions and determine the replacement frequency of the emulsion target. A precise characterization of this flux is therefore essential.

In this work, we report the muon flux measured in the central 31×31 cm² fiducial area of the detector using data from 2023 through 2025. The measured fluxes for **proton collisions** are: $(1.90 \pm 0.04) \times 10^{-2}$ nb/cm² (2023), $(3.74 \pm 0.06) \times 10^{-2}$ nb/cm² (2024), and $(2.48 \pm 0.04) \times 10^{-2}$ nb/cm² (2025).

The measured fluxes for **heavy-ion collisions** are $(3.13 \pm 0.11) \times 10^4$ nb/cm², $(5.54 \pm 0.17) \times 10^4$ nb/cm², and $(3.60 \pm 0.13) \times 10^4$ nb/cm² in 2023, 2024, and 2025, respectively. Uncertainties are dominated by systematic effects, with the statistical component contributing $\lesssim 1\%$ to the total uncertainty.

These results are in agreement with Monte Carlo predictions.

Keywords Muon flux · SND@LHC · CERN · LHC · Muon background

1 Introduction

The SND@LHC experiment [1] is designed to detect high-energy neutrinos in the forward pseudo-rapidity region $7.2 < \eta < 8.4$ produced by proton collisions at

IP1. The vast majority of observed events are from passing muons, which constitute the primary background to neutrino searches. Moreover, preventing excessive exposure of the emulsion films requires regular target replacement. The frequency of these replacements is directly dependent on the muon rate. Additionally, heavy-ion data further provides suitable conditions for studying detector response and tracking performance for low-energy muons. For these reasons, a precise measurement of the muon flux is essential.

We previously reported corresponding measurements for proton collisions in 2022 [2]. This paper gives an update for proton collisions and additional measurements for heavy-ion collisions in 2023, 2024 and 2025.

The muon flux is given by:

$$\Phi_\mu = \frac{N_{\text{tracks}}}{A \cdot \mathcal{L}_{\text{int}} \cdot \varepsilon} \quad (1)$$

where N_{tracks} is the number of muon tracks that traverse the effective detector area A used for the measurement, \mathcal{L}_{int} is the integrated luminosity at IP1 and ε is the tracking efficiency of the algorithm for the corresponding detector subsystem.

2 Detector and coordinate system

The SND@LHC detector [3] is a hybrid system featuring an ~ 830 kg target formed of tungsten plates interleaved with nuclear emulsion films and electronic trackers, which collectively function as an electromagnetic calorimeter (ECAL). The target is preceded by a veto system to tag charged particles originating from the IP1 direction, while a hadronic calorimeter (HCAL) and a muon system are situated downstream of the target (see Figure 1).

^ae-mail: ivaylo.dionisov@cern.ch

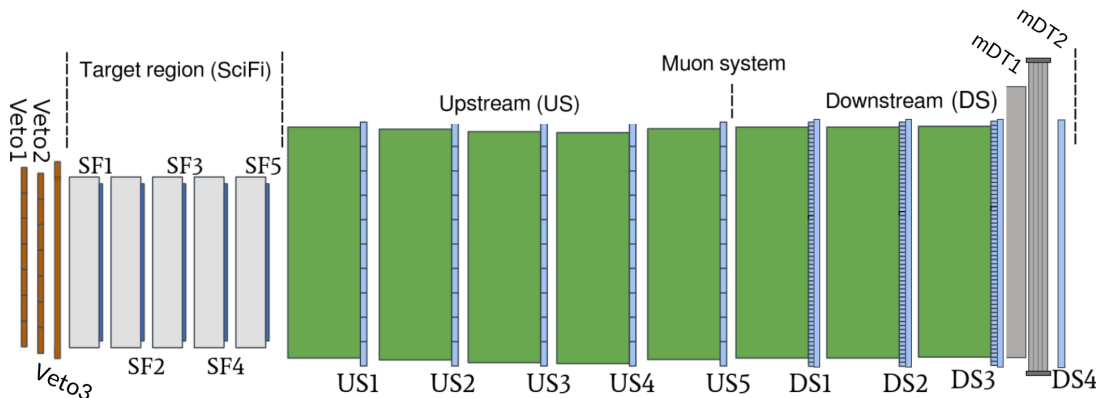


Fig. 1 Schematic side-view (YZ plane) of the SND@LHC detector layout (not to scale). The setup includes the third veto plane (installed in 2024) and the two mini-drift tube (mDT) planes (added in 2025).

Located in the TI18 tunnel, the detector is positioned approximately 480 m from the ATLAS interaction point along the collision axis. This location is shielded by the bending of charged particles originating from IP1 by the LHC magnets and the attenuation of neutral hadrons by 100 m of rock.

The veto system is made up of parallel planes of scintillator bars. Each layer consists of seven EJ-200 scintillator bars with dimensions of $42 \times 6 \times 1 \text{ cm}^3$ wrapped in aluminized mylar foil to prevent light leakage between adjacent bars. The horizontal scintillator bars are equipped with silicon photomultipliers (SiPMs) at both ends, whereas the vertical bars have SiPMs only at the top. To reduce the original inefficiency, the ground was excavated at the start of 2024 to lower the entire system, and a third veto plane was installed [4].

The target, serving as the vertex detector, comprise five walls of Emulsion Cloud Chambers (ECCs). In this work, however, the analysis is restricted to data recorded by the electronic detectors.

Interleaved with the target walls are the Scintillating Fiber (SciFi) tracker planes, which provide precise measurements of particle positions and electromagnetic shower energies. Each plane consists of two orthogonal layers (vertical and horizontal). Every layer is composed of three fiber mats, each measuring $13 \times 39 \text{ cm}^2$. The scintillating fibers have a diameter of $250 \mu\text{m}$ and are arranged in six staggered layers with a total thickness of 1.35 mm. The readout system utilizes SiPM multichannel arrays. Each mat is read out by four SiPMs with 128 channels of width $250 \mu\text{m}$, totaling 512 channels per mat and 1536 channels per plane. For this analysis, the planes are labeled SF1 to SF5, ordered from most upstream to most downstream.

The muon system consists of eight iron blocks and nine scintillator planes arranged alternately along the beam direction. The iron blocks, each 20 cm thick, serve

as the absorber material for the hadronic calorimeter (HCAL). The scintillator planes are categorized into two types: upstream (US) and downstream (DS).

The US system comprises the first five planes following the target region, labeled US1 to US5 in order of increasing distance from the target. Each plane is composed of ten horizontal scintillator bars with dimensions of $1 \times 6 \times 82.5 \text{ cm}^3$. These bars are read out by eight SiPMs at both ends, providing precise timestamps for traversing particles and measuring hadronic shower energy.

The DS system follows the US planes and offers finer granularity for muon identification and position measurement. DS planes consist of two orthogonal layers of scintillator bars (one horizontal and one vertical), except for the fourth plane (DS4), which contains only vertical bars. Each bar has a $1 \times 1 \text{ cm}^2$ cross-section, with lengths of 82.5 cm for horizontal bars and 63.5 cm for vertical bars. Horizontal bars are read out by a single SiPM at each end, while vertical bars are read out by a single SiPM at the top. Similarly to the SciFi, the DS planes are labeled DS1 to DS4.

Since 2025, the fourth DS plane has been relocated further downstream, with two drift tube planes (mDTs) installed between DS3 and DS4 to enhance muon tracking [5]. Data from the mDTs was not used for this analysis.

The system utilizes a triggerless data acquisition architecture, where all signals exceeding preset thresholds are processed by the front-end electronics and clustered in time to form events. An online software noise filter is subsequently applied. This maintains both a negligible detector deadtime and a negligible loss in signal efficiency. Events are recorded if they satisfy specific topological criteria, such as the presence of coincident hits across multiple detector planes.

Table 1 Beam attributes of heavy-ion and proton runs used for muon flux measurement with high-statistics track reconstruction. The given values are the date of the LHC fill, the energy per beam E , the bunch spacing t (time between bunches), the number of bunches per beam N , the crossing angle at IP1 and the integrated luminosities \mathcal{L}_{int} . For the 2025 proton data, the crossing angle is given as a range for 2025 proton data due to the introduction of crossing-angle anti-levelling [6], while fill 8695 lists the two specific values used. The uncertainty on the integrated luminosity is 3.5% for heavy ions and 2% for protons [7].

	Heavy-Ion Collisions						
	Date	E [GeV]	t [ns]	N	IP1 crossing angle [μrad]	Duration [h]	\mathcal{L}_{int} [μb^{-1}]
Fill 9232 (run 7080)	5 Oct 2023	6799	50	1123	170	11.0	61.01
Fill 9291 (run 7268)	22 Oct 2023	6799	50	1081	170	6.5	56.98
Fill 9312 (run 7329)	27 Oct 2023	6799	50	960	170	9.6	56.61
Fill 9317 (run 7346)	29 Oct 2023	6799	50	1080	170	8.2	57.85
Fill 10345 (run 10241)	9 Nov 2024	6800	50	1240	150	6.5	65.49
Fill 11318 (run 12589)	20 Nov 2025	6799	50	1240	150	8.6	115.82
	Proton Collisions						
	Date	E [GeV]	t [ns]	N	IP1 crossing angle [μrad]	Duration [h]	\mathcal{L}_{int} [μb^{-1}]
Fill 8695 (run 5888)	1 May 2023	6800	25	911	$-160/-135$	8.0	17.90×10^7
Fill 9606 (run 8329)	7 May 2024	6799	25	2352	150	14.4	53.24×10^7
Fill 10676 (run 11124)	31 May 2025	6799	25	2460	160-120	15.1	104.62×10^7

We employ a right-handed orthogonal coordinate system with its origin at 480 m from IP1 along the LHC beam collision axis (assuming a null crossing angle). The z -axis is oriented along the detector’s longitudinal axis, while the y -axis points upward, opposite to gravity.

3 Data and Monte Carlo simulations

3.1 Data sample

Each analyzed run corresponds to a specific LHC fill. For this study, full track reconstruction was performed on six runs from 2023 and two from 2024, utilizing both proton and heavy-ion data (where heavy ions specifically refer to fully stripped lead nuclei, $^{208}\text{Pb}^{82+}$). While reconstruction for 2025 was limited to representative subsamples, one proton and one heavy-ion run are included to facilitate a direct comparison with the 2023–2024 datasets. This is particularly relevant as 2025 saw the introduction of quasi-continuous crossing-angle anti-levelling, where the crossing angle is reduced as beam intensity decreases [6]. These runs are summarized in Table 1.

To investigate the time dependence of the muon flux, a sampling approach was adopted, analyzing a subset of events from selected runs throughout the data taking period, including the entirety of the analyzed 2025 data. For these runs, track reconstruction was performed on a small fraction of events, and the results were scaled to account for this subsampling. This approach is sufficient because the total uncertainty is

dominated by systematic effects rather than statistics, as detailed in Section 6. The luminosity for each LHC fill was provided by the ATLAS Collaboration [7].

3.2 Monte Carlo simulations

The simulation of the hadron collisions at the LHC interaction points is performed by CERN’s SY-STI team with the FLUKA Monte Carlo simulation package and the embedded external event generator DPMJET [8,9]. The resulting muons and charged hadrons are transported through the tunnel and rock to a virtual plane of dimensions $4.5 \times 4 \text{ m}^2$ located $\sim 35 \text{ m}$ upstream of the SND@LHC detector. Next, we use the output of this simulation to transport the particles to and through the detector with Geant4 [10].

The heavy-ion background was modeled by combining two distinct datasets: nuclear interactions (NI) from inelastic hadronic collisions and electromagnetic dissociation (EMD). These components are weighted according to their respective cross-sections to yield a total flux. So far, heavy-ion simulations were provided only for the 2022 LHC configuration.

4 Muon tracking with the electronic detectors

4.1 Track finding

The Hough transform algorithm [11] maps hits from the detector coordinate space into a parameter (Hough) space. Each hit corresponds to a curve in Hough space,

and the intersection of multiple curves identifies a common trajectory. By locating these intersections, the algorithm effectively groups hits to find candidate tracks.

4.2 Track fitting

Once a track is identified, it is reconstructed using the Kalman filter as implemented in the Genfit package [12, 13]. At SND@LHC, track reconstruction is done separately in the XZ and YZ planes, with the combination of which a 3D track can be constructed. The primary downside of this 3D track construction mechanism is the ambiguity that arises in the pairing process when multiple tracks are present. For this analysis, only single track events are considered, while multi-muon events, arising either from particle decays at IP1 or from muon interactions in the upstream rock, are excluded. This is justified by their scarcity (approximately $1/10^6$ for two muons and even less for three) and the fact that they are the subject of separate studies.

Track reconstruction requires hits in at least three planes, both horizontal and vertical. The Hough transform typically produces multiple candidate tracks, with the final track chosen as the one containing the highest number of hits. Since there are significant differences in the design and performance of the SciFi and DS components, tracking is done separately in the two subsystems.

4.3 Tracking efficiency

Tracking efficiency is estimated by identifying a “tagging track” in one of the two subsystems that extrapolate into the acceptance of the other one. Tracks found in the other system of tagged events are referred to as candidate tracks. A tag and candidate track pair are considered successfully matched if their extrapolated crossing points on a predefined reference plane between the two detectors lie within 3 cm of each other. The efficiency is then calculated as the ratio of matched pairs to the total number of tagging tracks.

A fiducial region of uniform efficiency is defined for both SciFi and DS measurements and is shown in Figure 2. The efficiencies are summarized in Table 2.

5 Angular distribution

Given the detector’s considerable distance from IP1, it is anticipated that most tracks will exhibit minimal slopes. However, the angular distribution depicted in Figure 3 reveals a secondary peak at approximately

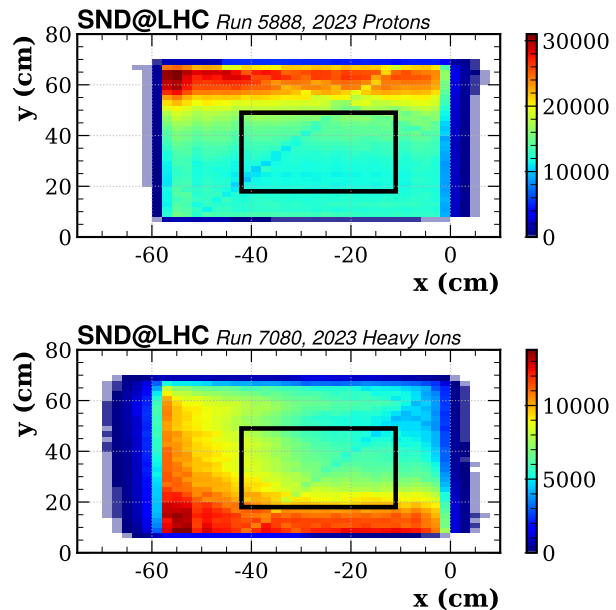


Fig. 2 DS Hough transform track density distribution at $z = 430$ cm in data. Higher density is observed at the upper part for proton collisions and in the lower part for heavy-ion collisions. The box illustrates the fiducial region of uniform efficiency for both SciFi and DS tracking. The diagonal lines of lower occupancy are artifacts of the 2D binning.

Table 2 Comparison of tracking efficiency across the two detector subsystems. Fluctuations between years and bunch types (protons vs. heavy ions) reflect variations in the muon energy spectra and the energy-dependent nature of tracking performance. Quoted uncertainties are derived from the variance within the defined fiducial region.

SND@LHC Run	SciFi Efficiency	DS Efficiency
<i>2023 Data</i>		
5888 (Protons)	0.949 ± 0.007	0.923 ± 0.011
7080 (Heavy Ions)	0.923 ± 0.015	0.884 ± 0.024
<i>2024 Data</i>		
8329 (Protons)	0.912 ± 0.009	0.920 ± 0.014
10241 (Heavy Ions)	0.855 ± 0.015	0.854 ± 0.019
<i>2025 Data</i>		
11124 (Protons)	0.922 ± 0.001	0.924 ± 0.001
12589 (Heavy Ions)	0.895 ± 0.003	0.880 ± 0.003

$\theta_{XZ} \approx 45$ mrad in the horizontal projection, alongside a plateau near 110 mrad. Monte Carlo simulations suggest that this secondary peak corresponds to low-energy muon tracks, which are more numerous during heavy-ion runs.

A positive angle corresponds to muons traveling away from the LHC’s center. Extrapolating from the detector to its intersection with the LHC ring places the deflection or production source approximately 60 m upstream. The GIS portal map [14] identifies two

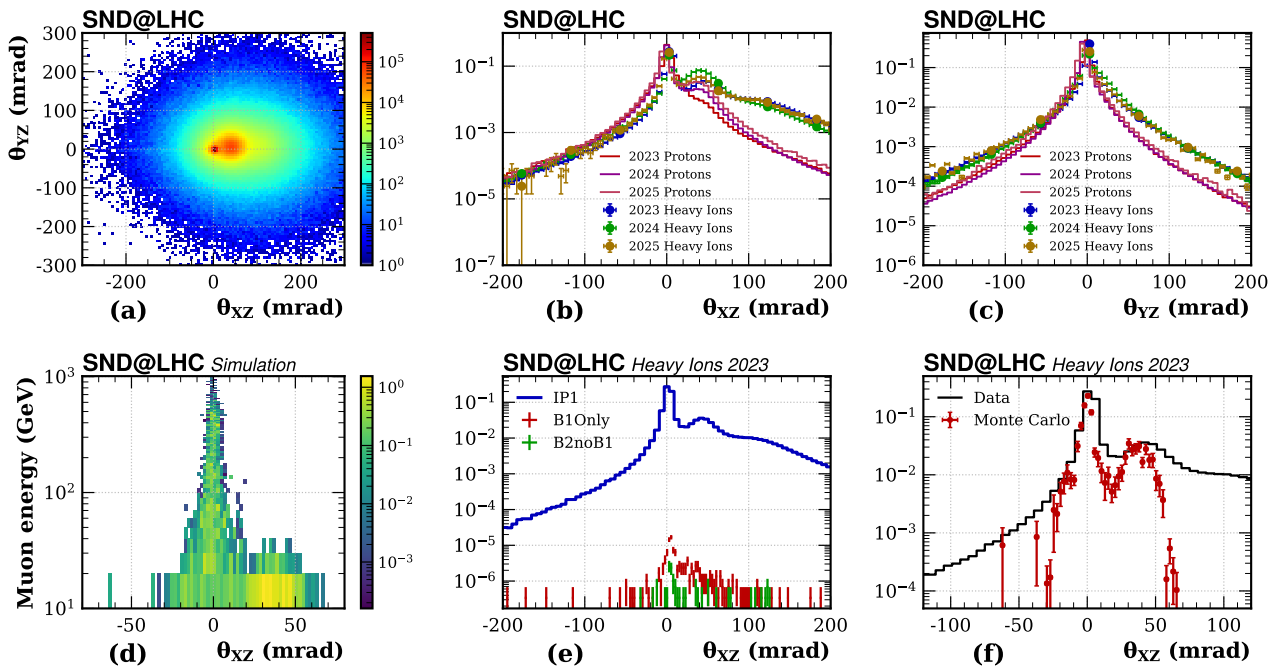


Fig. 3 Track angle distributions and source separation. Panel (a) is in total counts, while panels (b, c, e, f) are normalized to unit area. Panel (d) shows a 2D histogram of track angle versus muon energy for heavy-ion simulations in arbitrary units. The labels IP1, B1Only, and B2noB1 denote events coincident with an IP1 collision, a non-colliding beam 1, or a non-colliding beam 2 bunch slot, respectively. Contributions from non-colliding beams are negligible and are excluded from the final muon flux results.

LHC elements at this distance: the quadrupole magnet MQ.11R1 and the empty cryostat LEHR.11R1, as shown on Figure 4. FLUKA simulations provide insights into the muon origin before reaching the virtual plane. Initially, pions and kaons are generated by heavy-ion interactions at the LEHR.11R1 site. Subsequently, these particles decay into muons, whose trajectories are directed to the detector by the quadrupole magnet MQ.11R1 and following dipoles. The muon production points in the simulation are given in Figure 5.



Fig. 4 The LHC elements LEHR.11R1 and MQ.11R1. Pions and kaons, generated through ion interactions at LEHR.11R1, decay into muons. These muons are subsequently directed toward the detector by the quadrupole magnet MQ.11R1 and following dipoles.

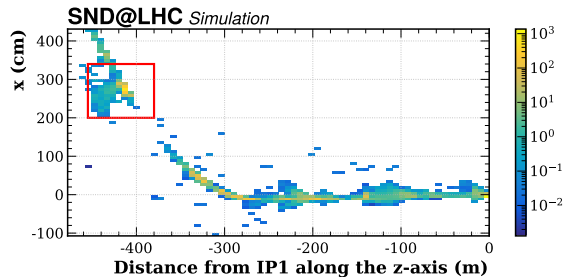


Fig. 5 Muon production distribution along the beamline in heavy-ion simulations. The coordinate system is centered at IP1 with the z -axis pointing along the beam collision axis, away from SND@LHC. Concentration of muon production within the boxed area, approximately 415 m from IP1, aligns with the position of the LHC half-cell 11.

6 Muon flux

The fiducial area for both subsystems has been chosen with boundaries of $-42 \text{ cm} \leq X \leq -11 \text{ cm}$ and $18 \text{ cm} \leq Y \leq 49 \text{ cm}$. Muon flux contributions from non-IP1 meson decays originating 60 m upstream of the detector cannot be isolated and are thus included in the final results. The independent measurements from the the two subsystems, along with the weighted average,

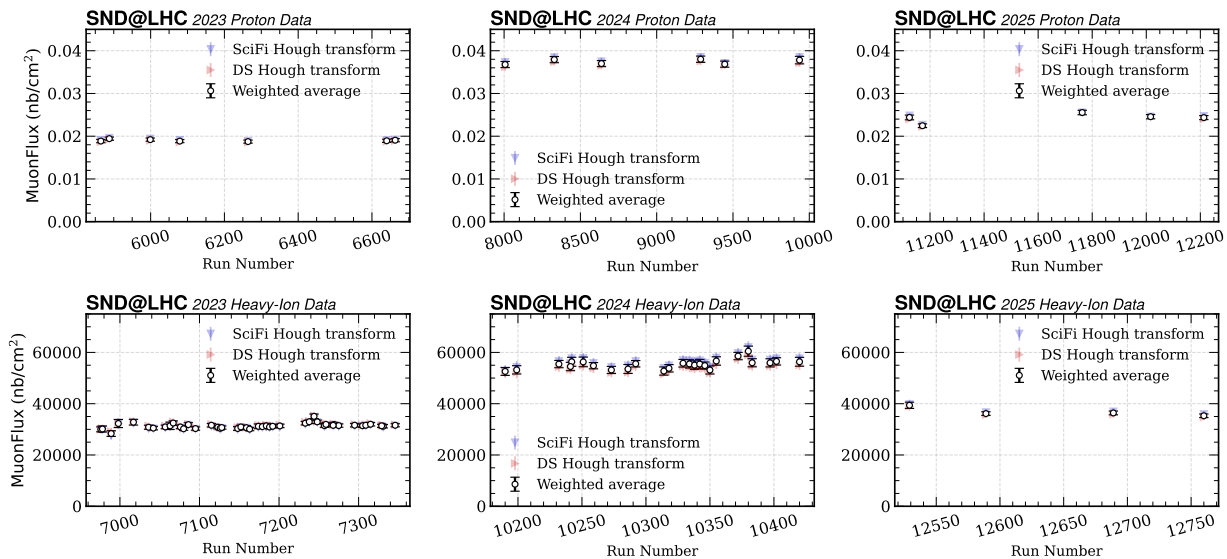


Fig. 6 Muon flux measurement across all SND@LHC runs that correspond to LHC fills with production-mode filling schemes.

Table 3 Measured and simulated muon fluxes for the 2023–2025 periods. Relative contributions to the total uncertainty are provided for each measurement. The 2022 proton flux results are taken from Ref. [2].

Dataset	Muon Flux	Uncertainty breakdown (% contribution to variance)		
		Statistics	Efficiency	Luminosity
<i>Heavy-Ion Collisions (10^4 nb/cm²)</i>				
Data (2023)	3.13 ± 0.11	0.01	7.53	92.46
Data (2024)	5.54 ± 0.17	0.08	22.40	77.52
Data (2025)	3.60 ± 0.13	0.06	8.76	91.18
Monte Carlo (2022)	2.99 ± 0.09	96.70	3.30	N/A
<i>Proton Collisions (10^{-2} nb/cm²)</i>				
Data (2023)	1.90 ± 0.04	0.37	11.25	88.38
Monte Carlo (2023)	1.67 ± 0.05	94.71	5.29	N/A
Data (2024)	3.74 ± 0.06	1.26	36.85	61.89
Monte Carlo (2024)	3.34 ± 0.12	87.88	12.12	N/A
Data (2025)	2.48 ± 0.04	1.35	33.11	65.54
Monte Carlo (2025)	3.13 ± 0.14	87.21	12.79	N/A
Data (2022)	2.06 ± 0.12	8.33	91.67 (Combined Systematics)	

are presented in Figure 6, where it can be seen that it stays constant over time.

The muon flux results for heavy-ion and proton data from 2023 to 2025 are summarized in Table 3. No heavy-ion data was collected in 2022 due to the decision to conclude the run two weeks early to mitigate the European energy crisis [15]. Heavy-ion collision simulations were only provided with the 2022 machine configuration.

For proton data, the observed flux deviates from predictions by 10% to 20%. Given the complexity of the simulations, from the collision generator to the propagation through rock of varying composition, with cumulative uncertainties at each stage, this level of agreement can be considered excellent.

6.1 LHC configurations

The significant increase in muon flux by a factor of ~ 2 between 2023 and 2024 can be attributed to changes in the LHC configuration [16]. Most notably, the LHC IR1 triplet polarity was reversed in 2024, inverting the quadrupole sequence from Focus-Defocus-Focus (FDF) to Defocus-Focus-Defocus (DFD) to optimize the machine lifetime and Run 3 performance. For heavy-ion operations, the amplitude of the bound-free pair production (BFPP) orbit bumps was also adjusted to prevent magnet quenching under these new settings. As a result, an increased number of TeV-energy muons reached the detector.

In 2025, the nominal settings were restored, but the crossing angle at IP1 was set to the horizontal plane. This configuration resulted in a muon flux $\sim 23\%$ higher than in 2023 for proton collisions ($\sim 13\%$ for heavy ions). The detailed analysis is part of a separate study and is not addressed here.

7 Conclusion

We have reported the muon flux measurements for heavy-ion and proton collisions at the SND@LHC experiment using data collected between 2023 and 2025. Muons originating from beam interactions at LEHR.11R1 follow the same trajectory as IP1 muons and are synchronous with collision events. Consequently, they cannot be temporally separated and are included in the reported flux values.

The measured muon fluxes for heavy-ion collisions are:

$$\mathbf{2023\ Data:} \quad \Phi_{\mu} = (3.13 \pm 0.11) \times 10^4 \text{ nb/cm}^2 \quad (2a)$$

$$\mathbf{2024\ Data:} \quad \Phi_{\mu} = (5.54 \pm 0.17) \times 10^4 \text{ nb/cm}^2 \quad (2b)$$

$$\mathbf{2025\ Data:} \quad \Phi_{\mu} = (3.60 \pm 0.13) \times 10^4 \text{ nb/cm}^2 \quad (2c)$$

The measured muon fluxes for proton data are:

$$\mathbf{2023\ Data:} \quad \Phi_{\mu} = (1.90 \pm 0.04) \times 10^{-2} \text{ nb/cm}^2 \quad (3a)$$

$$\mathbf{2024\ Data:} \quad \Phi_{\mu} = (3.74 \pm 0.06) \times 10^{-2} \text{ nb/cm}^2 \quad (3b)$$

$$\mathbf{2025\ Data:} \quad \Phi_{\mu} = (2.48 \pm 0.04) \times 10^{-2} \text{ nb/cm}^2 \quad (3c)$$

Systematic uncertainties dominate, with the statistical component contributing approximately 1% for proton data and $\lesssim 0.1\%$ for heavy-ion data (see Table 3). Unlike the 2022 proton data analysis, a unified fiducial area was adopted for both SciFi and DS measurements. This consistency eliminates the choice of detector subsystem as a source of systematic uncertainty.

A comparison with Monte Carlo simulations shows agreement within $\sim 10\%$ for the 2023 and 2024 proton data, and within $\sim 20\%$ for the 2025 data. Heavy-ion simulations were performed using the 2022 LHC configuration. Given the similarities between the 2022 and 2023 heavy-ion LHC configurations, these simulations show good agreement ($\sim 5\%$) with the 2023 experimental results.

References

1. R. Albanese, et al., “*Observation of collider muon neutrinos with the SND@LHC experiment*”, *Phys. Rev. Lett.* **131**, 031802 (2023). doi:10.1103/PhysRevLett.131.031802
2. R. Albanese, et al., “*Measurement of the muon flux at the SND@LHC experiment*”, *Eur. Phys. J. C* **84**, 90 (2024). doi:10.1140/epjc/s10052-023-12380-3
3. G. Acampora, et al., “*SND@LHC: the scattering and neutrino detector at the LHC*”, *JINST* **19**, P05067 (2024). doi:10.1088/1748-0221/19/05/P05067
4. D. Abbaneo, et al., “*Installation and performance of the 3rd Veto plane at the SND@LHC detector*”, *JINST* **20**, P07011 (2025). doi:10.1088/1748-0221/20/07/P07011
5. L. Mozzina, “*Upgrade of the SND@LHC muon detectors with drift tubes*”. Master’s thesis, Università di Bologna (2025). URL <https://amslaurea.unibo.it/id/eprint/36655/>
6. H. Timko, et al., “*Highlights from the LHC*”, in *PoS*, vol. EPS-HEP2025, (2025), p. 007. doi:10.22323/1.485.0007
7. ATLAS Collaboration, “*Preliminary analysis of the luminosity calibration for the ATLAS 13.6 TeV data recorded in 2023*”. Tech. Rep. ATL-DAPR-PUB-2024-001, CERN (2024). URL <https://cds.cern.ch/record/2900949>
8. G. Hugo, et al., “*Status and advances of Monte Carlo codes for particle transport simulation*”, *EPJ Nuclear Sci. Technol.* **10**, 20 (2024). doi:10.1051/epjn/2024023
9. S. Roesler, R. Engel, J. Ranft, “*The Monte Carlo Event Generator DPMJET-III*”, in *Advanced Monte Carlo for Radiation Physics*, (Springer Berlin Heidelberg, 2001), pp. 1033–1038. doi:10.1007/978-3-642-18211-2_166
10. S. Agostinelli, et al., “*Geant4—a simulation toolkit*”, *Nucl. Instrum. Meth. A* **506**, 250 (2003). doi:10.1016/S0168-9002(03)01368-8
11. P.V.C. Hough, “*Machine Analysis of Bubble Chamber Pictures*”, in *Conf. Proc. C*, vol. 590914, (1959), pp. 554–558
12. R.E. Kalman, “*A New Approach to Linear Filtering and Prediction Problems*”, *J. Basic Eng.* **82**(1), 35 (1960). doi:10.1115/1.3662552
13. J. Rauch, T. Schlüter, “*GENFIT — a Generic Track-Fitting Toolkit*”, *J. Phys.: Conf. Ser.* **608**, 012042 (2015). doi:10.1088/1742-6596/608/1/012042
14. CERN. “*CERN GIS Portal*”. <https://gis.cern.ch/>. Accessed: 2025-09-18
15. D. Jacquet, et al., “*The LHC Run 2022*”, in *Proc. IPAC*, (2023), pp. 551–554. doi:10.18429/JACoW-IPAC2023-MOPL020
16. T. Persson, et al., “*LHC optics commissioning in 2023 and 2024*”, in *Proc. IPAC*, (2024), pp. 67–70. doi:10.18429/JACoW-IPAC2024-MOPC12

Acknowledgements We acknowledge the support for the construction and operation of the SND@LHC detector provided by the following funding agencies: CERN; the Bulgarian Ministry of Education and Science within the National Roadmap for Research Infrastructures 2020–2027 (object CERN) and for the support of this study under the National Program “Young Researchers and Postdoctoral Students - 2”; ANID FONDECYT grants No. 3230806, No. 1240066, 1240216 and ANID - Millenium Science Initiative Program - ICN2019_044 (Chile); the Deutsche Forschungsgemeinschaft (DFG, ID 496466340); the Italian National Institute for Nuclear Physics (INFN); JSPS, MEXT, the Global COE program of Nagoya University, the Promotion and Mutual Aid Corporation for Private Schools of Japan for Japan; the National Research Foundation of Korea with grant numbers 2021R1A2C2011003, 2020R1A2C1099546, 2021R1F1A1061717, and 2022R1A2C100505; Fundação

para a Ciência e a Tecnologia, FCT grant numbers CEECIND/01334/2018, CEECINST/00032/2021 and PRT/BD/153351/2021 (Portugal), CERN/FIS-INS/0028/2021; the Swiss National Science Foundation (SNSF); TENMAK for Turkey (Grant No. 2022TEN-MAK(CERN) A5.H3.F2-1). J.C. Helo Herrera and O. J. Soto Sandoval acknowledge support from ANID FONDECYT grants No.1241685 and 1241803. M. Climescu, H. Lacker and R. Wanke are funded by the Deutsche Forschungsgemeinschaft (DFG, German Research Foundation), Project 496466340. This research was financially supported by the Italian Ministry of University and Research within the Prin 2022 program.

We express our gratitude to our colleagues in the CERN accelerator departments for the excellent performance of the LHC. We thank the technical and administrative staff at CERN and at other SND@LHC institutes for their contributions to the success of the SND@LHC efforts. We are particularly grateful to the CERN SY-STI team for their expertise regarding beam losses and for providing dedicated simulations of the orbit bump tests, which were critical to understanding the background conditions. We also thank our colleagues in the CERN BE-ABP group for the insightful discussions on LHC configurations. We thank Luis Lopes, Jakob Paul Schmidt and Maik Daniels for their help during the construction.

The SND@LHC Collaboration

D. Abbaneo⁹, S. Ahmad^{4,2}, R. Albanese^{1,2}, A. Alexandrov¹, F. Alicante^{1,2}, F. Aloschi^{1,2},
 K. Androsov⁶, A. Anokhina³, L.G. Arellano^{1,2}, C. Asawatangtrakuldee³⁸, M.A. Ayala Torres^{27,32},
 N. Bangaru^{1,2}, C. Battilana^{4,5}, A. Bay⁶, C. Betancourt⁷, D. Bick⁸, R. Biswas⁹, A. Blanco Castro¹⁰,
 V. Boccia^{1,2}, M. Bogomilov¹¹, D. Bonacorsi^{4,5}, W.M. Bonivento¹², P. Bordalo¹⁰, A. Boyarsky^{13,14},
 S. Buontempo¹, T. Camporesi^{10,48}, V. Canale^{1,2}, D. Centanni¹, F. Cerutti⁹, A. Cervelli⁴,
 V. Chariton⁹, M. Chernyavskiy³, A. Chiuchiolo²¹, K.-Y. Choi¹⁷, F. Cindolo⁴, M. Climescu^{18,46},
 G.M. Dallavalle⁴, N. D'Ambrosio⁴⁵, D. Davino^{1,20}, R. De Asmundis¹, P.T. de Bryas⁶, G. De Lellis^{1,2,9},
 M. de Magistris^{1,16}, G. Del Giudice^{1,2}, G. De Marzi²¹, A. De Roeck²⁶, S. De Pasquale²¹, A. De Rújula⁹,
 M.A. Diaz Gutierrez⁷, A. Di Crescenzo^{1,2}, C. Di Cristo^{1,2}, D. Di Ferdinando⁴, C. Dinc²³, I. Dionisov¹¹,
 R. Donà^{4,5}, O. Durhan^{23,43}, D. Fasanella⁴, O. Fecarotta^{1,2}, M. Ferrillo⁷, A. Fiorillo^{1,2}, N. Funicello²¹,
 R. Fresa^{1,24}, W. Funk⁹, G. Galati¹⁵, K. Genovese^{1,24}, V. Giordano⁴, A. Golutvin²⁶, E. Graverini^{6,41},
 C. Guandalini⁴, L. Guiducci^{4,5}, A.M. Guler²³, V. Guliaeva³⁷, G.J. Haefeli⁶, C. Hagner⁸,
 J.C. Helo Herrera^{27,40}, E. van Herwijnen²⁶, S. Ilieva^{9,11}, S.A. Infante Cabanas^{27,40}, A. Infantino⁹,
 A. Iuliano^{1,2}, A.M. Kauniskangas⁶, E. Khalikov³, S.H. Kim²⁹, Y.G. Kim³⁰, G. Klioutchnikov^{1,2},
 M. Komatsu³¹, N. Kononova³, S. Kuleshov^{27,32}, H.M. Lacker¹⁹, I. Landi^{1,2}, O. Lantwin^{1,47},
 F. Lasagni Manghi⁴, A. Lauria^{1,2}, K.Y. Lee²⁹, K.S. Lee³³, W.-C. Lee⁸, V.P. Loschiavo^{1,20},
 A. Mascellani⁶, M. Majstorovic⁹, F. Mei⁵, A. Miano^{1,44}, A. Mikulenko¹³, M.C. Montesi^{1,2},
 D. Morozova^{1,2}, L. Mozzina^{4,5}, F.L. Navarria^{4,5}, W. Nuntiyakul³⁹, K. Obayashi³⁴, S. Ogawa³⁴,
 N. Okateva³, M. Ovchynnikov⁹, G. Paggi^{4,5}, A. Perrotta⁴, D. Podgrudkov³, N. Polukhina^{1,2},
 F. Primavera^{4,49}, A. Prota^{1,2}, A. Quercia^{1,2}, S. Ramos¹⁰, A. Reghunath¹⁹, T. Roganova³,
 F. Ronchetti⁶, N. Rossolino^{1,16}, T. Rovelli^{4,5}, O. Ruchayskiy³⁵, T. Ruf⁹, Z. Sadykov¹, M. Samoilo³,
 V. Scalerà^{1,16}, W. Schmidt-Parzefall⁸, O. Schneider⁶, G. Sekhniadze¹, A. Serban⁹, N. Serra⁷,
 M. Shaposhnikov⁶, V. Shevchenko³, T. Shchedrina^{1,2}, L. Shchutska⁶, H. Shibuya^{34,36}, C. Silano^{1,21},
 G.P. Siroli^{4,5}, G. Sirri⁴, T. E. Smith^{1,2}, G. Soares¹⁰, J.Y. Sohn²⁹, O.J. Soto Sandoval^{27,40},
 M. Spurio^{4,5}, N. Starkov³, J. Steggemann⁶, A. Tarek⁹, J. Tesarek⁹, I. Timiryasov³⁵, V. Tioukov¹,
 C. Trippi⁶, E. Urso¹⁹, G. Vankova-Kirilova¹¹, G. Vasquez^{9,27}, V. Verguilov¹¹, N. Viegas Guerreiro
 Leonardo^{10,28}, C. Vilela¹⁰, R. Wanke¹⁸, S. Yamamoto³¹, Z. Yang⁶, C. Yazici^{1,2}, S.M. Yoo¹⁷,
 C.S. Yoon²⁹, E. Zaffaroni⁶, J. Zamora Saá^{27,32}

¹Sezione INFN di Napoli, Napoli, 80126, Italy

²Università di Napoli "Federico II", Napoli, 80126, Italy

³Affiliated with an institute formerly covered by a cooperation agreement with CERN

⁴Sezione INFN di Bologna, Bologna, 40127, Italy

⁵Università di Bologna, Bologna, 40127, Italy

⁶Institute of Physics, EPFL, Lausanne, 1015, Switzerland

⁷Physik-Institut, UZH, Zürich, 8057, Switzerland

⁸Hamburg University, Hamburg, 22761, Germany

⁹European Organization for Nuclear Research (CERN), Geneva, 1211, Switzerland

¹⁰Laboratory of Instrumentation and Experimental Particle Physics (LIP), Lisbon, 1649-003, Portugal

¹¹Faculty of Physics, Sofia University, Sofia, 1164, Bulgaria

¹²Università degli Studi di Cagliari, Cagliari, 09124, Italy

¹³University of Leiden, Leiden, 2300RA, The Netherlands

¹⁴Taras Shevchenko National University of Kyiv, Kyiv, 01033, Ukraine

¹⁵Sezione INFN di Bari, Università degli Studi di Bari Aldo Moro, Bari, 70124, Italy

¹⁶Università di Napoli Parthenope, Napoli, 80143, Italy

¹⁷Sungkyunkwan University, Suwon-si, 16419, Korea

¹⁸Institut für Physik and PRISMA Cluster of Excellence, Mainz, 55099, Germany

¹⁹Humboldt-Universität zu Berlin, Berlin, 12489, Germany

²⁰Università del Sannio, Benevento, 82100, Italy

²¹Dipartimento di Fisica 'E.R. Caianello', Salerno, 84084, Italy

²³Middle East Technical University (METU), Ankara, 06800, Turkey

²⁴Università della Basilicata, Potenza, 85100, Italy

²⁵Pontifical Catholic University of Chile, Santiago, 8331150, Chile

²⁶Imperial College London, London, SW72AZ, United Kingdom

²⁷Millennium Institute for Subatomic physics at high energy frontier-SAPHIR, Santiago, 7591538, Chile

²⁸Departamento de Física, Instituto Superior Técnico, Universidade de Lisboa, Lisbon, Portugal

²⁹Department of Physics Education and RINS, Gyeongsang National University, Jinju, 52828, Korea

³⁰Gwangju National University of Education, Gwangju, 61204, Korea

³¹Nagoya University, Nagoya, 464-8602, Japan

³²Center for Theoretical and Experimental Particle Physics, Facultad de Ciencias Exactas, Universidad Andrés Bello, Fernandez Concha 700, Santiago, Chile

³³Korea University, Seoul, 02841, Korea

³⁴Toho University, Chiba, 274-8510, Japan

³⁵Niels Bohr Institute, Copenhagen, 2100, Denmark

³⁶Present address: Faculty of Engineering, Kanagawa, 221-0802, Japan

³⁷Constructor University, Bremen, 28759, Germany

³⁸Department of Physics, Faculty of Science, Chulalongkorn University, Bangkok, 10330, Thailand

³⁹Chiang Mai University, Chiang Mai, 50200, Thailand

⁴⁰Departamento de Física, Facultad de Ciencias, Universidad de La Serena, La Serena, 1200, Chile

⁴¹Also at: Università di Pisa, Pisa, 56126, Italy

⁴²Affiliated with Pakistan Institute of Nuclear Science and Technology (PINSTECH), Nilore, 45650, Islamabad, Pakistan ⁴³Also at: Atilim University, Ankara, Turkey

⁴⁴Affiliated with Pegaso University, Napoli, Italy

⁴⁵Affiliated withg Laboratori Nazionali del Gran Sasso, L'Aquila, 67100, Italy

⁴⁶Now at: Ghent University, Ghent, Belgium

⁴⁷Now at: Siegen University, Siegen, Germany

⁴⁸Also at: Boston University and Georgian Technical University ⁴⁹Now at: Sezione INFN di Padova, Università degli Studi di Padova, Padova, 35122, Italy